

С 344.1и

С-57

ОБЪЕДИНЕННЫЙ  
ИНСТИТУТ  
ЯДЕРНЫХ  
ИССЛЕДОВАНИЙ

Дубна

E13 - 3141



ЛАБОРАТОРИЯ  
ВЫСОКИХ ЭНЕРГИЙ

I.V. Chuvilo, P.I. Filipov, A.S. Gavrilov,  
N.N.Govorun, I.A. Golutvin, E.D. Gorodnichev,  
I.I. Ivanchenko, S.S. Kirilov, Yu.T. Kiryushin,  
V.D. Kondrashov, G.M. Kadykov,  
V.I. Moroz, T.C. Nigmanov, O.K. Nefedyev,  
V.P. Pugachevich, V.N. Sadovnikov,  
E.N. Tsyganov, Yu.V. Zanevsky

FILMESS SPARK CHAMBER SYSTEM FOR  
OPERATION WITH ON-LINE COMPUTER

1967.

E13 - 3141

4786/1  
28

**I.V. Chuvilo, P.I. Filipov, A.S. Gavrilo,  
N.N.Govorun, I.A. Golutvin, E.D. Gorodnichev,  
I.I. Ivanchenko, S.S. Kirilov, Yu.T. Kiryushin,  
V.D. Kondrashov, G.M. Kadykov,  
V.I. Moroz, T.C. Nigmanov, O.K. Nefedev,  
V.P. Pugachevich, V.N. Sadovnikov,  
E.N. Tsyganov, Yu.V. Zanevsky**

**FILMESS SPARK CHAMBER SYSTEM FOR  
OPERATION WITH ON-LINE COMPUTER**

A system of wire spark chambers used on-line with the computer BESM-3M has been designed for experiments performed using Dubna synchrophasotron beams. The system consists of nine spark chambers with magnetostrictive readout each permitting to measure X and Y coordinates of sparks, of a 1 km datalink and the computer.

Spark chambers have been tested in a 4.7 GeV/c negative pion beam. The momentum distribution of negative pions scattered on a hydrogen target at an angle of  $\geq 10$  mrad has been measured, which corresponds to the momentum transferred of  $\sqrt{t} > 47$  MeV/c.

Spark chambers, data acquisition electronics, datalink to the computer are shortly described. The results of testing in the pion beam are reported.

## I. Spark Chambers

Wire spark chambers with magnetostrictive readout have been described in refs. <sup>(1-3)</sup>. The principle of such spark chamber operation is seen from fig. 1. Schematically shown in fig. 1 are two wire electrodes ( X and Y ), all the wires of each are connected together at one side. Thin magnetostrictive strips are located perpendicular to wires forming electrodes in the near vicinity to them. At each end of the magnetostrictive strips there are receiving coils. The strip edges are coated with rubber dampers (D). Receiving coils are put in the polarizing magnet field (M).

When a spark breakdown occurs in the chamber, a pulse goes through the corresponding wires of X and Y electrodes at the

point A . The current magnetic field causes pulses of longitudinal elastic deformation in X and Y strips which propagate in both the directions at a speed  $V = 5000$  M/sec. When a deformation pulse passes through a receiving coil, the magnetic permeability of the strip inside the coil is changed (the inverse magnetostrictive effect) consequently, the magnetic flux is also varied. The change of the magnetic flux induces a voltage signal in the receiving coil. Thus, by measuring time intervals between the spark breakdown in the chamber and the appearance of voltage pulses on the corresponding receiving coils, the spark coordinates of  $X_1$  ,  $X_2$  and  $Y_1$  ,  $Y_2$  can be measured.

In the case of one spark the following conditions should hold in the chamber:

$$X_1 + X_2 = \text{const.} \quad \text{and} \quad Y_1 + Y_2 = \text{const.},$$

which makes it possible to easily separate events when only a single spark occurred in the chamber and also to improve the accuracy of spark localization.

Fig. 2 shows the pictures of spark chambers having the sensitive electrode area of  $200 \times 200 \text{ mm}^2$  and  $480 \times 480 \text{ mm}^2$ . Spark chamber electrodes are made of copper wire 0.1 mm in diameter, the winding step being 1 mm. The wires of one electrode are located perpendicular to those of the other one. Magnetostrictive strips of the 50% Fe + 50% Co alloy (0.1 mm x 1 mm in cross section) are isolated from electrode wires with mylar  $200 \mu\text{k}$  thick. The distance between the electrodes is  $8 \pm 0.03$  mm. The chamber volume is separated from the external volume with mylar  $100 \mu\text{k}$  thick. The chambers have two gas leads-in through which they are blown with operating gas (75% Ne , 25% He and 1.5%  $\text{C}_2\text{H}_5\text{OH}$  mixture).

The chamber consists of three parts: X and Y electrodes and a separating frame. These parts of the chamber are made of epoxy with quartz filling by casting in vacuum. This method provides high accuracy of the construction and a good identity of the chambers.

## 2. Data Acquisition System

The block-diagram of the data acquisition system is shown in fig.3. It has 36 similar channels converting time intervals into pulse numbers.

Signals from 36 receiving coils of spark chambers (4 for each chamber) are propagated along 15 m cables to gating shapers-amplifiers. The amplifiers are closed normally and are opened only for  $150 \mu\text{sec}$  in  $10 \mu\text{sec}$  after triggering the system.

The clock generator is triggered by the signal from coincidence circuits and starts generating pulses at a repetition rate about  $10^7 \text{p/sec}$  in  $15 \mu \text{sec}$  after a triggering pulse. Pulses from the input of this generator are sent to ten bit binary counters via the corresponding gate  $G_1$ .

A pulse from the pertinent shaper-amplifier upsets the flip-flop T, which closes the gate  $G_1$  and the contents of the binary scaler is, thus, proportional to the value of the corresponding coordinate. The amplifier control of signals from spark chambers, the check of coincidence circuit dead time and information transfer to the computer are performed by means of the control system. Information from scalers is transformed by using a shift register to be transmitted to the computer. The error of coordinate measurement due to the detection system is also not larger than 0.5 mm.

## 3. Datalink and Data Handling in the On-Line Computer

Nowadays the system is used to study negative pion elastic scattering on protons in the momentum range 2-8 GeV/c at angles of 10-40mrad.

Fig. 4 shows the experimental arrangement. A liquid hydrogen target 50 cm long was used, the total wall thickness along the beam being 0.4 mm of mylar.

SC-1-7 spark chambers are  $200 \times 200 \text{ mm}$  large and serve to measure a pion scattering angle at the target. Using spark chambers SC -8-9  $480 \times 480 \text{ mm}^2$  large the pion momentum is measured by its deviation in the field of the analysing magnet M.

The experiment is run 1 km from the computer. Information from the detection system is transmitted on cable in the subsequent code. The datalink operates at  $10^6$  pulse/sec repetition rate.

All information obtained at each spark chamber triggering is combined in a series of nine 45-bit words. The series transmission time is 1 msec. The information of 300 spark chamber triggerings can be sent to the computer memory each accelerator burst. The information is analysed during the period between accelerator bursts (about 8 sec) and the results are recorded on magnetic tape.

During data accumulation on magnetic tape they are preliminary processed and the whole system operation is checked up. On an operator inquiring the chamber efficiency, the number of breakdowns on old tracks, double spark triggerings and also data on coordinate, angular and momentum beam distributions can be printed out.

The data are processed according to the following algorithms.

1. Two straight lines are drawn basing on the data obtained with spark chambers in front and behind the target. The information is selected from chambers where there are sparks lying outside the particle track.
2. The intersection angle of these lines is determined and the coordinates of the point are found where the straight lines were at the shortest distance.
3. The scattered particle momentum is found for the events of scattering at an angle larger than 10 mrad.

The processing programme is used in various operation modes permitting the machine to print necessary hystograms, and thus, to more accurately check the whole process of experimental performance.

#### 4. Performance Tests

Spark chambers triggered on average 100 times per accelerator burst. The dead time of the spark chamber system was 4.2 msec. The chamber efficiency was about 97% (the inefficiency of spark chambers and the dead time were, due, mainly, to the pulse supply system).

Fig. 5 shows the distribution of the negative pion number versus the scattering angle in the case of an empty target. The root-mean-square value of the scattering angle is about 0.9 mrad and is determined, mainly, by multiscattering in air.

Fig. 6 shows the same dependence for a full target.

Fig. 7 shows the momentum distribution of the beam used in the experiment.

Fig. 8 shows the same dependence after improving the beam magnetic system.

Fig. 9 shows the distribution of negative pion scattering events at an angle larger than 10 mrad at the Z coordinate  $Z_m = 250$  cm.

The momentum distribution of negative pions scattered at an angle  $\theta \geq 10$  mrad and having the coordinate of the interaction point  $Z = 180-340$  cm is shown in fig. 10. As is seen from the fig, there is an elastic  $\pi^-p$ -scattering peak in the distribution. Peak dispersion and its position are the same as in the negative pion momentum distribution (see fig. 10 and 7). The background contribution is 10-15%. As many as 100000 primary negative pion tracks were analysed in running the experiment.

## 5. Characteristics of the System

Below is given a list of the basic system properties.

### Spark chambers

Dimensions: a) SC1-SC7 -  $200 \times 200$  mm<sup>2</sup>

b) SC8-SC9 -  $480 \times 480$  mm<sup>2</sup>

Gap - 8 mm.

Each chamber has  $1.5 \times 10^{-3}$  radiation length (t).

The accuracy of coordinate measurement is  $\pm 0.6$  mm.

Inefficiency, including breakdowns on the old track is about 10%.

Memory time is about 1  $\mu$ sec.

### Data acquisition system

Counting value - 0.5 mm.

Error in determining the coordinates due to the detection system - 0.5 mm.

Detection time - 120  $\mu$ sec.

The maximum number of events transferred to the computer memory per accelerator burst - 300.

In conclusion the authors wish to express their gratitude to N.I. Mashkevich for help in arranging the experiment and preparing some units of the system, Yu.T. Borzunov, L.B. Golovanov and Dr. A.G. Zeldovich for making the target, to T.B. Avericheva, V.S. Evtisov, E.K. Kuryatnikov, A. Karpunin and M.N. Mikhailova, O.N. Tsislak, V.N. Sutulin, A.F. Elishev for help in constructing the system and running the experiment.

### R e f e r e n c e s

1. V. Perez-Mendez and J.M. Pfab. Nuclear Instr. and Meth., 33, 141 (1965).
2. S. Miyamoto. Nuclear Instr. and Meth., 35, 323 (1965).
3. A.S. Gavrilov, I.A. Golutvin, Yu.V. Zanevsky, S.S. Kirilov, B.A. Kulakov, L.G. Makarov, E.N. Tsyganov. Preprint - 2398, Dubna. 1966; PTE No. 5 (1966).

Received by Publishing Department  
on January 25, 1967.

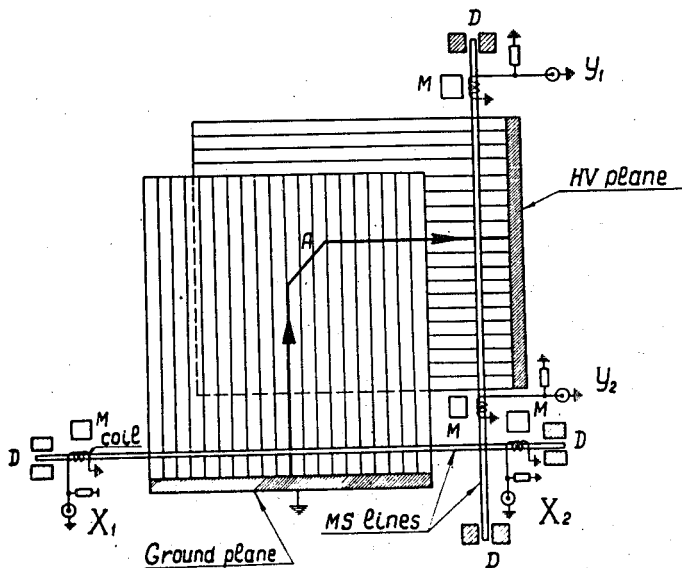


Fig. 1. Principles of magnetostrictive spark chamber operation. RC-receiving coils, D-dampers, M-polarizing magnets.

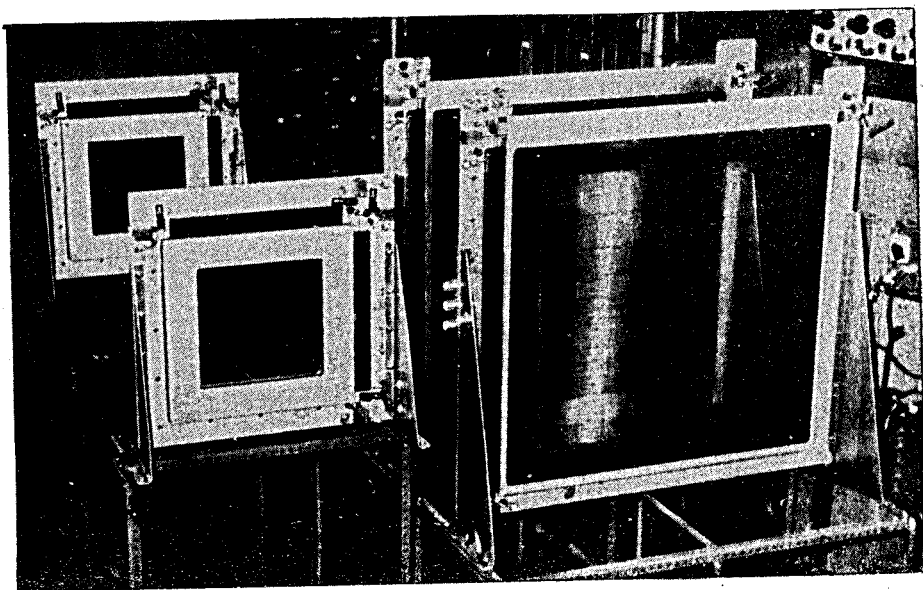


Fig. 2. Spark chambers of two types used in the experiment.

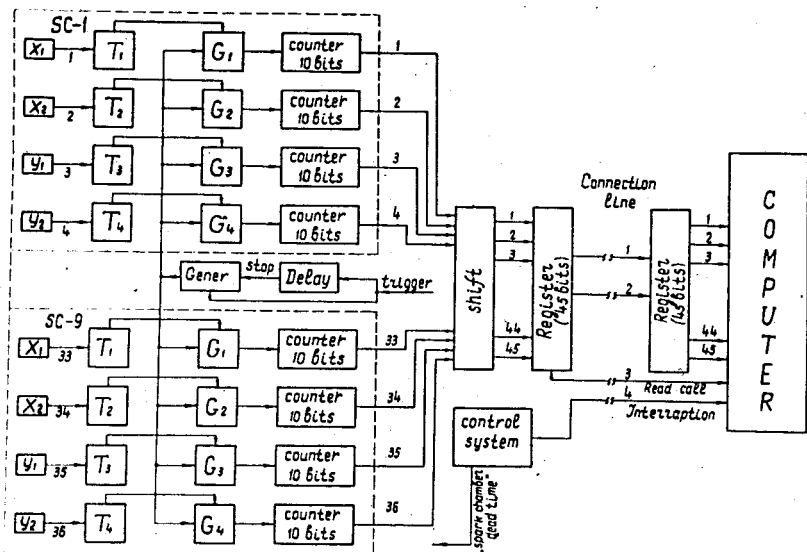


Fig. 3. Block-diagram of the detection system.  $X_1$ ,  $X_2$ ,  $Y_1$ ,  $Y_2$  - amplifiers of signals from the appropriate coils of the spark chamber,  $T_1$ ,  $T_2$ ,  $T_3$ ,  $T_4$  -triggers controlled by the appropriate gates,  $G_1$ ,  $G_2$ ,  $G_3$ ,  $G_4$  -gates.

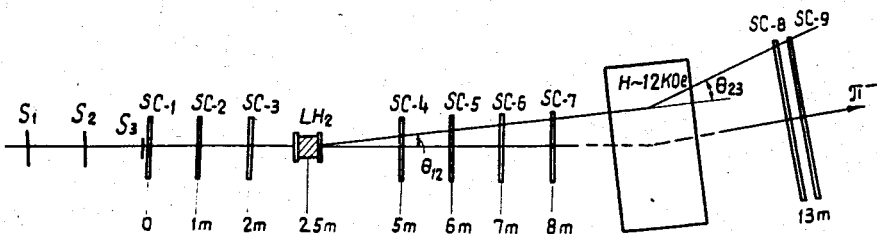
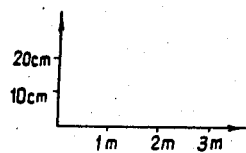


Fig. 4. Experimental arrangement,  $C_1$ ,  $C_2$ ,  $C_3$  -scintillation counters triggering the system; SC -1 - SC -9 - magnetostrictive spark chambers,  $LH_2$  -liquid hydrogen target,  $H$  -analysing magnet,  $\theta_{1,2}$  -particle scattering angle,  $\theta_{2,3}$  -angle of particle deflection in the magnetic field.

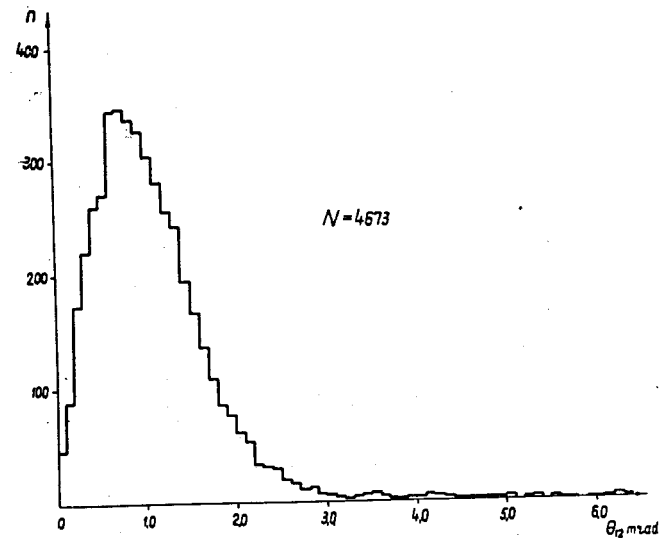


Fig. 5.  $\theta_{1,2}$  -distribution for non-interacting particles in the case of a full target.

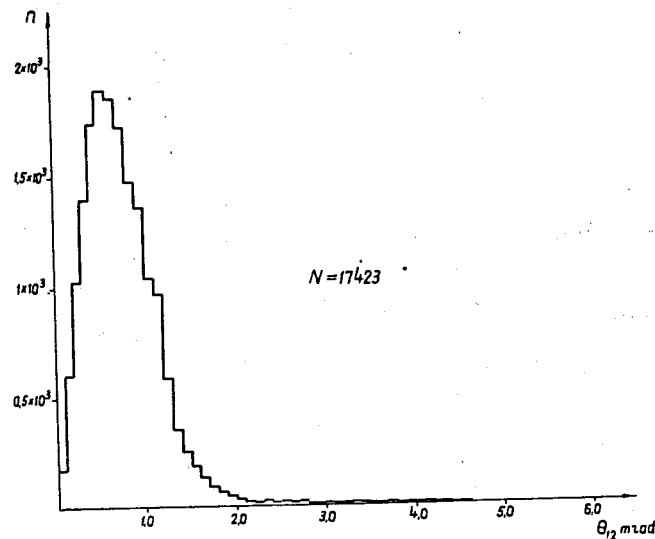


Fig. 6.  $\theta_{1,2}$  -distribution for non-interaction particles in the case of an empty target.

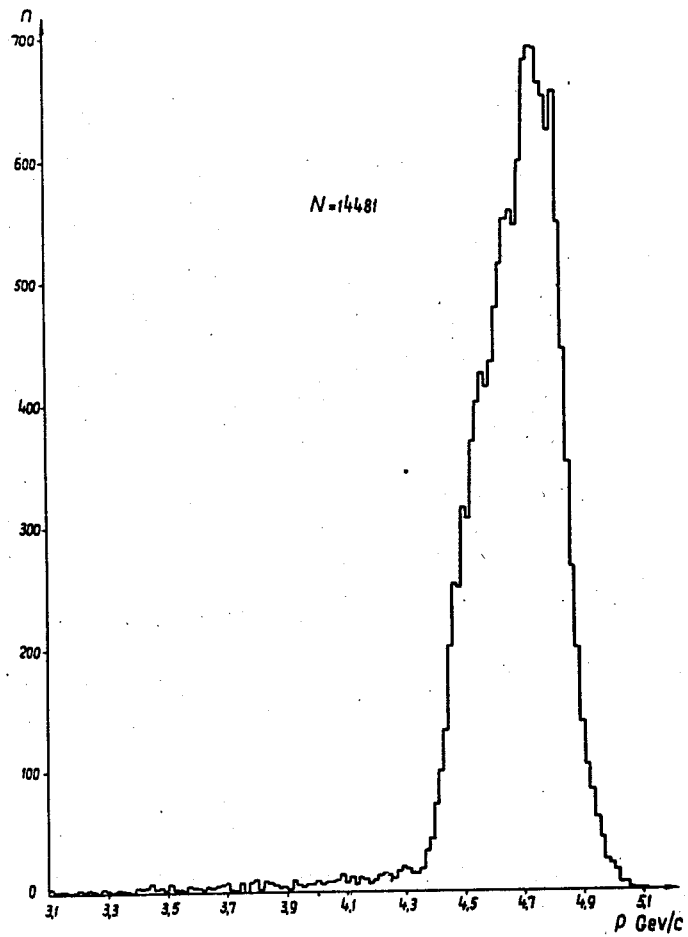


Fig. 7. Momentum distribution of the beam used in the experiment.

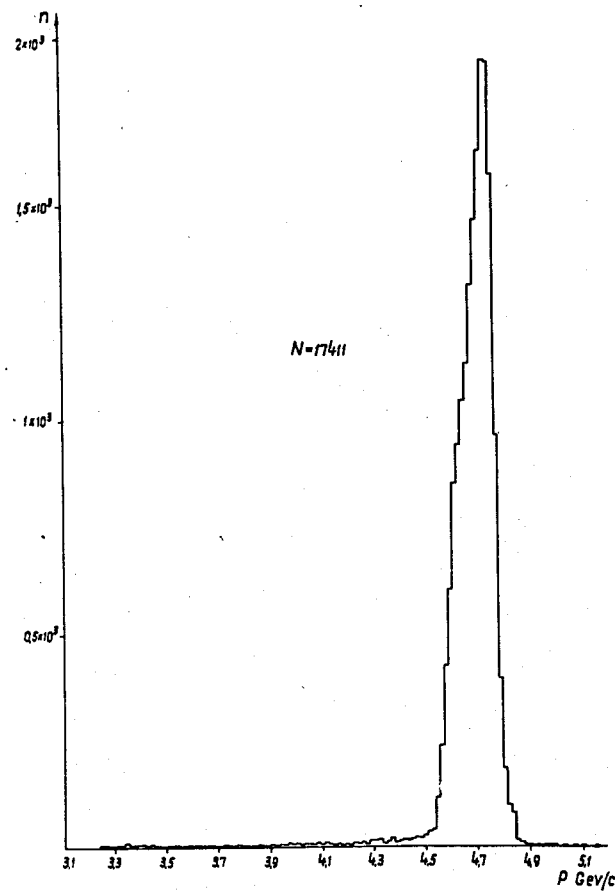


Fig. 8. Momentum distribution of the beam after improving the magnetic system of the channel.

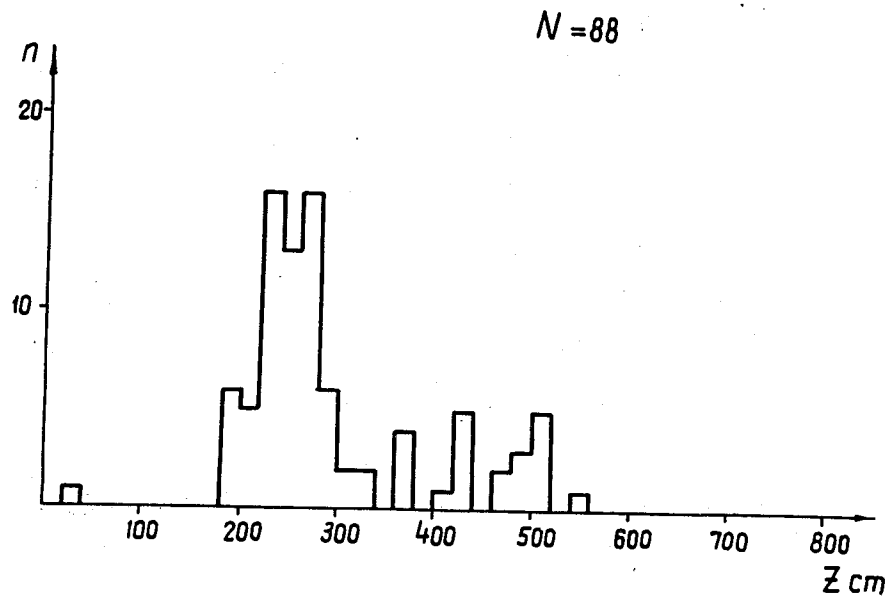


Fig. 9. Distribution of scattering events at an angle  $\theta_{1,2} > 10$  mrad at the Z coordinate (along the beam) of the scattering point.

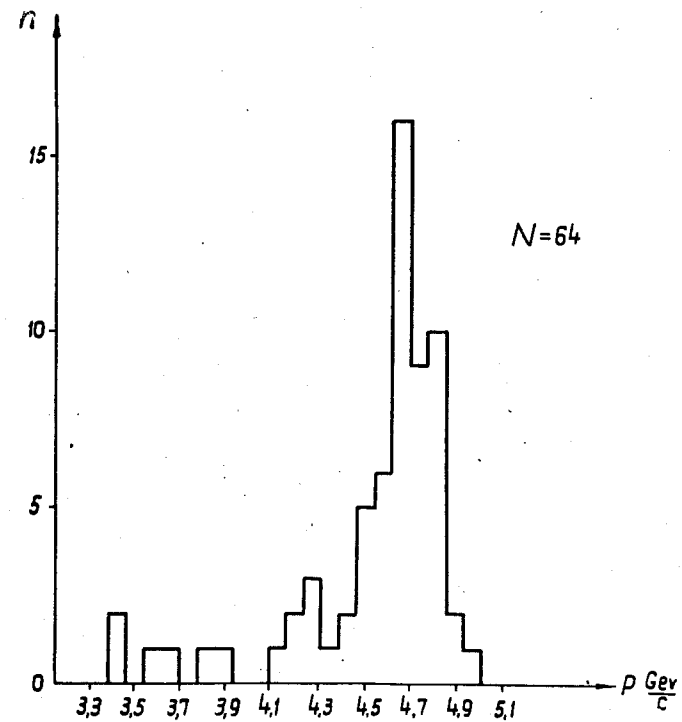


Fig. 10. Momentum distribution of secondary particles for scattering events at angles of  $\theta_{1,2} \geq 10$  mrad for which the coordinate lies in the target region.